Investigating the Geometry and Mechanical Properties of Human Round Window Membranes Using Micro-Fringe Projection

*Junfeng Liang, *Don Nakmali, *Rong Z. Gan, †Hongbing Lu, and *Chenkai Dai

*School of Aerospace and Mechanical Engineering, University of Oklahoma, Norman, Oklahoma; and †Department of Mechanical Engineering, University of Texas at Dallas, Richardson, Texas

Hypothesis: The geometry and the mechanical property of the round window membrane (RWM) have a fundamental impact on the function of cochlea.

Background: Understanding the mechanical behavior of RWM is important for cochlear surgery and design for the cochlear implant. Although the anatomy of RWM has been widely studied and described in the literature, argument remains regarding the true shape of RWM. The mechanical properties of RWM are also scarcely reported due to the difficulty of the measurement of the small size RWM.

Methods: In this paper, micro-fringe projection was used to reconstruct the 3-dimensional geometries of 14 RWMs. Mechanical properties of the RWMs were subsequently measured using finite element (FE) model and an inverse method. The three-dimensional surface topographies and the

curvatures of the two major directions reconstructed from the micro-fringe projection both demonstrated wide variations among samples.

Results: The diameters of the RWMs vary from 1.65 to $2.2 \,\mathrm{mm}$ and the curvatures vary from -0.97 to $3.76 \,\mathrm{mm}^{-1}$. The nonlinear elasticity parameters in the Ogden model for each sample was measured and the average effective Young's modulus is approximately $1.98 \,\mathrm{MPa}$.

Conclusion: The geometries and mechanical properties of the human RWM measured in the work could potentially be applied to surgery design and on modeling analysis for the cochlea. **Key Words:** Finite element method—Human round window—Inverse method—Micro-fringe projection.

hearing rehabilitation of patients suffering from mixed,

Otol Neurotol 41:xxx-xxx, 2020.

Round window (RW) is one of the two openings from the middle ear into the cochlea. When the acoustic vibration enters the cochlea through the oval window, the round window membrane (RWM) works as a valve, balancing the pressure of the fluid in the cochlea by vibrating with an opposite phase to the vibration of oval window membrane (1–3). Because RWM can play an even larger role for transmission of sound to the inner ear than the tympanic membrane, it was called as secondary tympanic membrane (4).

Clinically, the RW has been commonly used as a portal for electrode insertion for cochlear implant (5). The anatomical and topographical knowledge about the round window region determines a successful insertion of the electrode in the cochlea implant surgeries. In addition to insertional implantation, floating mass transducer (FMT) placed at the RWM is another feasible option for the

conductive, and sensorineural hearing loss. Several clinical studies have been conducted to investigate the effect of different coupling methods (6,7). While the best coupling technique and material for stimulating the RWM remain undetermined (8–10), these studies show that the attachment and RWM mechanical properties directly affect the efficiency of the function of FMT. For both clinical practices, a thorough knowledge of anatomical intricacies and the properties pertaining to the RWM is a must to obtain desirable excellency in the surgical results.

Additionally, the geometries and the mechanical properties of RWM are also important for modeling the middle ear or cochlea function, especially with finite element (FE) models. Due to lack of accurate information of the geometries and mechanical properties, most of the authors assume the RWM as a flat ellipse shape and with the same mechanical properties of some other tissues (11–13). Although these models are able to simulate experimental data, their geometrical parameters are not closely related to anatomical or physiological properties. Knowledge of real RWM morphology and the accurate measurement of the mechanical properties of RWM are critical for establishing highly realistic FE models for the analysis of the human ear.

The authors disclose no conflicts of interest.

DOI: 10.1097/MAO.0000000000002911

© 2020, Otology & Neurotology, Inc.

Address correspondence and reprint requests to Chenkai Dai, M.D., Ph.D., chool of Aerospace and Mechanical Engineering, University of Oklahoma, Engineering Laboratory Rm. 114, Norman, OK 73019; E-mail: chenkaidai@ou.edu

This work is funded by DOD W81XWH-14-1-0228, NIH R01DC011585, DOD W81XWH-13-MOMJPC5-IPPEHA, and NSF CMMI-1636306, CMMI-1661246, and CMMI-172043.

To date, there are only a few data on mechanical properties of RWM reported in the literature, probably due to the difficult measurements on such a small size and fragile tissue. Volume-pressure properties of RWM on human temporal bone were first described by Ivarsson and Pedersen (14). They observe the change of the volume concealed by the RWM and the cochlear under the pressure up to 20 cm H₂O. Elastic properties of human RWM were then measured by Ishii et al. (15) using a force sensor needle system, where a RWM was stretched by the needle and the elastic modulus was determined with the needle force and the stretch ratio of the RWM. Ishii et al. (15) did not consider the change of elastic modulus at large deformation (hyperelastic effect). Recently, dynamic properties were measured by Zhang and Gan (16) on human and Gan et al. (17) on chinchilla in situ using the laser Doppler vibrometry (LDV). In their study, the RWM was forced to vibrate with a speaker and the LDV laser was used to measure the vibration velocity. In the latter two studies, the material properties were determined indirectly using an inverse method, (i.e., the material parameters were found by fitting model predictions with experimental results), where the complex geometry of RWM was not considered.

Here, we presented our study on the geometries and mechanical properties of the RWM using a micro-fringe projection technique. The RWM was fully exposed in the human temporal bone, and micro-fringe projection was used to capture the geometry and displacement of RWM driven by static pressures. FE model on each RWM was established. An inverse method was used to determine the hyperelastic properties of RWM. This study is expected to fill the gap of material properties of RWM in situ and provides information on RWM for future highly realistic human ear FE modeling.

METHODS

Sample Preparation

Fourteen RWM samples from fresh human cadaver temporal bones (eight left and six right) obtained through the Life Legacy Foundation were used in this study. All donors were free from the history of ear diseases associated with the RWM and the average age of the donors was 70 (ranging from 46 to 79, four men and six women). The protocol has been approved by the U.S. Army Medical Research (USAMR) and Material Command Office of Research Protections (MCORP). Before the measurement, a temporal bone was trimmed into a bony block with a dimension of about 25 mm × 25 mm × 25 mm, containing the intact cochlea. The bony structure in the middle ear was first removed by a cut parallel to the RW to fully expose the round window niche from the medial side (Fig. 1A). Using the stapes as a reference, the bony structure of the cochlea was carefully trimmed until RWM could be seen from the cochlea

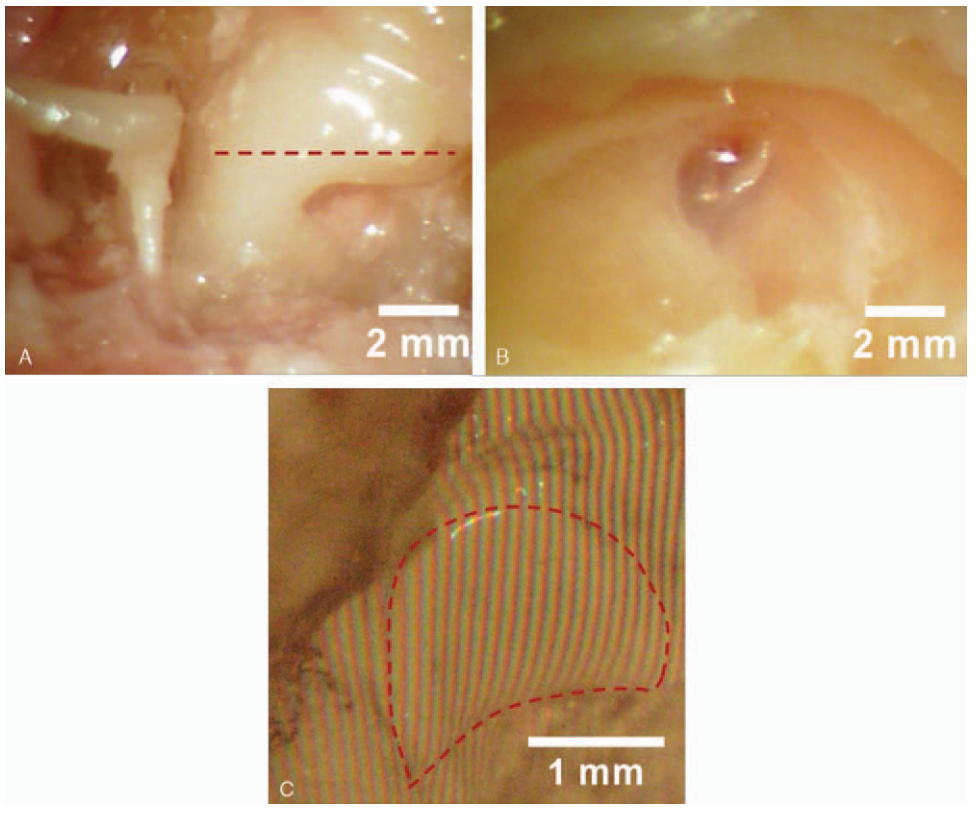


FIG. 1. Sample preparation for the round window membrane: (*A*) Front view. The red line shows the location where the cut was applied to expose the round window membrane from the cochlea side. (*B*) Back view. The RWM exposed from the cochlea side. (*C*) The RWM painted with titanium oxide and projected with micro-fringes. The black dash line outlines the boundary of the RWM. RWM indicates round window membrane.

side. The RWM was investigated and samples that with damage RWM were excluded from the study. A tubing of 75 mm long with 1.25 mm diameter was inserted into the RW and sealed airtight with two-part epoxy (Gorilla Glue, Inc.). Note that mucoperiosteal folds or "false round window membranes" (false RWM) developed in the nearby promontory of RW are commonly found to seal the RW niche. In case the false RWM existed in the RW, a sharp needle was used to puncture the false RWM to avoid the possibility of blockading the air passage to the RWM. Subsequently, the RWM was painted with a thin layer of titanium oxide in saline (100 mg/ml) to give a better reflection for the micro-fringe projection. To maintain compliance and hydration of the soft tissue during the sample preparation and experiment, the RWMs were moisturized with a droplet of 0.9% saline every 15 minutes. Figure 1B shows an image of the typical temporal bone acquired by a CCD camera through a microscope in this study.

Experimental Procedure

Figure 2 shows the schematic diagram of the experimental setup. A micro-fringe projection system was used to determine the deformed surface topography of the RWM under a prescribed static pressure (Fig. 1C). In fringe projection, a set of grating with pitch density of 20 cycles/mm (Edmund Optics, Dwyer Instruments, Inc., Barrington, USA) was projected onto the RWM and the image of the projected fringe on the surface of the object was acquired by a digital camera (Nikon D7000; Nikon Inc., Melville, USA). Another image of fringe projected onto a reference plane under the same setup was also acquired. The image of the projected fringes on the RWM was subsequently digitally superimposed with the image of projected fringes on the reference plane to generate interferometry (18,19). The surface profile of the RWM was then determined by the virtual interferometry using a five-step-shifting method (18,19). Note that the RWM is small with boundary covered by painting. To accurately reconstruct the geometry of the RWM, two images, one of RWM under no pressure and one under pressure were superimposed to find the fixed points along the boundary of the RWM.

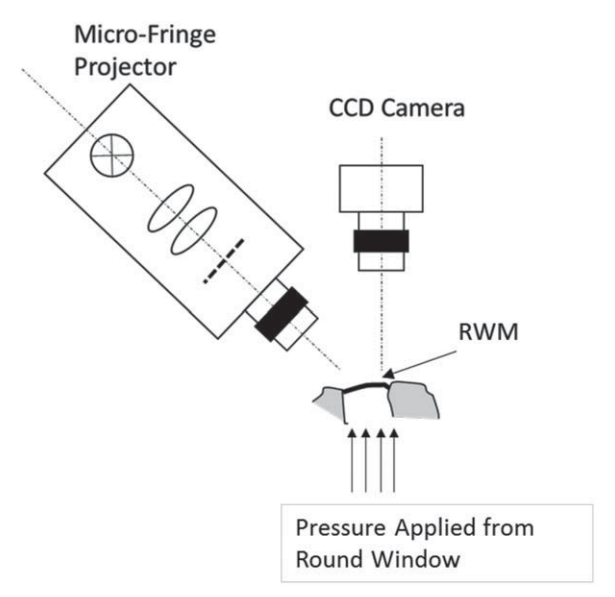


FIG. 2. Schematic of measurement setup with micro-fringe projection and applied pressure.

During the measurement, the sample was placed on a gimbal holder attached to a temporal bone bowl mounted on an XYZ stage. This setup allowed the direction of the RWM surface to be adjusted for the micro-fringe projection and for the observation by a camera. A pressure monitor system was used to apply pressures on the RWM from the round window either positive (bulging) or negative (vacuuming) values. The system consists of two three-way stopcocks, a 20 ml syringe, and a water manometer with a resolution of 2.5 mm water bar (Dwyer Instruments, Inc. Series 1235). One of the three-way stopcocks served as a valve to control the pressures applied on the RWM; it allowed releasing pressure for the whole system, applying pressure to the specimen, and locking up the pressure in the temporal bone block. Another three-way stopcock was used to switch between positive pressure and negative pressure applied on the RWM. Before the measurement, each sample was preconditioned by applying a pressure value of 1 kPa for five cycles to allow the RWM to reach a steady state. Stepwise pressures with increments of ± 0.125 kPa up to ± 1.0 kPa were applied through a tube into the lateral side of the RWM and monitored with the manometer. The resting time between each step was approximately 2 seconds and the total time of the measurement was approximately 2 minutes. Surface profiles of the RWMs under different pressures were acquired and the corresponding volume displacements of the RWMs were calculated. The detail of surface profile reconstruction can be found in our previous publications (20,21).

Inverse Method

The mechanical properties of the RWM were determined with an inverse method. The measurement of each RWM sample was simulated in FE models using ANSYS 18. The surface topography under the normal state, reconstructed from the micro-fringe projection, was converted to a three-dimensional model using the computer-aided design (CAD) software, SolidWorks 2017. Since the RWM thickness is small compared with its major or minor axis, it was modeled as a shell with a thickness of 70 µm (22,23) in ANSYS. The RWM was characterized as a hyperelastic material with material behavior similar to that of an elastomer. The niche of the RWM was fixed for all degrees of freedom (no translations or rotations). The dimensions of the RWMs samples were shown in Table 1. For each individual sample, the volume displacement was simulated under static pressures according to those applied to the RWM in the experiment.

Ogden model was used as the constitutive material model to describe the mechanical behavior of RWM under large deformation. The tangent modulus, E_t , is described as:

$$E_{t} = \frac{dT_{U}}{d\varepsilon_{U}}$$

$$= \sum_{i=1}^{N} \frac{2\mu_{i}}{\alpha_{i}} [(\alpha_{i} - 1)(1 + \varepsilon_{U})^{\alpha_{i} - 2} + (0.5\alpha_{i} + 1)(1 + \varepsilon_{U})^{-0.5\alpha_{i} - 2}], i = 1, 2$$

$$(1)$$

where, T_U is the uniaxial stress, ε_U is the uniaxial strain, and α_i and μ_i are the material parameters. The constitutive material parameters were determined through an iteration procedure such that the difference of the volume displacements between the experiment and simulation was minimized (20,21). Subsequently, the Young's modulus of RWM was calculated by linearly curve fitting the tangent modulus at the strain below 10%.

TABLE 1. Dimensions and material parameters of RWM in 14 human temporal bones measured with micro-fringe projection

Sample	Curvature (mm ⁻¹)		Length (mm)			Material Properties			
	Short	Long	Short	Long	Area (mm ²)	μ_1 (MPa)	α_1	μ_2 (MPa)	α_2
TB-15-41	-0.67	0.38	1.97	2.04	3.15	0.40	0.66	0.48	0.89
TB-15-40	0.60	0.51	1.83	2.20	3.16	0.41	1.16	0.44	0.91
TB-15-39	0.35	-0.50	1.91	2.04	3.05	0.46	1.24	0.27	1.03
TB-15-36	-0.71	0.31	1.88	2.04	3.01	0.39	1.04	0.47	1.30
TB-15-35	0.30	-1.64	1.75	2.07	2.85	0.41	0.83	0.44	0.95
TB-15-33	0.66	-1.06	1.79	2.00	2.80	0.45	0.89	0.46	1.19
TB-15-32	0.86	1.10	1.76	2.09	2.89	0.36	1.11	0.37	0.96
TB-15-31	-0.97	0.62	1.89	1.87	2.77	0.58	0.99	0.40	1.11
TB-15-30	-0.43	0.31	1.65	2.14	2.78	0.41	1.16	0.44	0.91
TB-15-28	0.41	0.07	1.74	2.03	2.78	0.45	0.97	0.35	1.01
TB-15-27	0.35	-0.18	1.83	1.99	2.86	0.44	1.14	0.43	1.08
TB-15-26	-0.42	0.32	1.74	2.04	2.78	0.39	0.88	0.36	1.15
TB-15-25	0.58	3.76	1.77	1.92	2.67	0.28	1.13	0.42	1.19
TB-15-17	2.64	2.98	1.79	2.10	2.95	0.34	1.03	0.42	1.05
Mean	0.67	1.60	1.81	2.04	2.89	0.43	1.02	0.42	1.04
SD	1.95	4.21	0.08	0.08	0.14	0.06	0.15	0.06	0.17

RWM indicates round window membrane.

RESULTS

Figure 3 demonstrates the 3D surface reconstructions of the 14 RWMs under the zero-pressure state. The z-direction in the figure indicates the direction from the lateral (middle ear) side to the medial (inner ear) side. The boundary of each RWM is outlined and drawn in Figure 3 above the 3D surface. A comparison between FE simulated and the experimental measured surface profile of a typical RWM sample under three different pressures are also plotted in Figure 3 at three selected cross-sections. The average difference is about 5%, which validates our FE simulation.

The measured 3D surfaces demonstrate patterns that are reported from existing literature: the boundary of RWM is generally not round but appears close to ellipse or cashew shape with a long axis and a short axis. The curvature of a RWM is not necessarily unidirectional but in some cases show both positive (convex) and negative values (concave) depending on the in-plane direction. The plane of the anterior and the inferior section of the RWM is found to be more out-of-plane, while the posterior and superior section is more in-plane positioned. Additionally, the superior section often profiles an unbroken arch while the inferiorly section forms a more complicated shape. The 3D surfaces of RWM also exhibit significant varieties of geometry, which are seemly influenced by the variances of RW boundaries anatomy (24,25). Lastly, different geometries were also found between left and right ear for individuals.

To investigate the convexity of the RWM, the curvatures along long axis and short axis were calculated by fitting the curves along these two axes with circular functions. The curvatures of the 14 RWMs along the

two axes are listed in Table 1, where a positive value indicates the RWM is convex toward cochlea and a negative value indicates it is concave toward cochlea. It shows that the curvature along the two axes of the RWM can be either in identical or opposite directions. Nevertheless, most of the samples show inverse convexity along the two axes. These results agree with the saddle shape of RWM reported in previous literatures (26,27).

The average size of the longest axis of the human RWM is found to be 2.04 mm (min, 1.87; max, 2.20; SD, 0.08). The smallest diameter, assessed perpendicular to the longest axis (mostly near the RWMs mid-portion), is 1.81 mm (min, 1.65; max, 1.97; SD, 0.08). The mean area of the RWM is found to be 2.89 mm² and varied between 2.77 and 3.16 mm² (SD, 0.14). The data of the diameters are given in Table 1.

Similar to the typical loading-displacement in a tensile test, the relationship between pressure and volume displacement is used to describe the mechanical response of the RWMs. Figure 4 shows the pressure as a function of the volume displacement of the 14 RWMs. The pressure-volume displacement curves exhibit strong nonlinearity. Sharing the same features of other soft tissue such as tympanic membrane, the increase of volume displacement significantly slows down as the pressure rises up. This indicates that the RWM is a hyperelastic material, i.e., the material becomes stiffer as the stress increase. However, compared with that of the tympanic membrane, volume displacements of RWM show no significant difference between negative and positive pressures. This can be due to the lower convexity of the RWM compared with the tympanic membrane. The symmetry of volume-displacement over positive/ negative pressures is consistent with that was observed

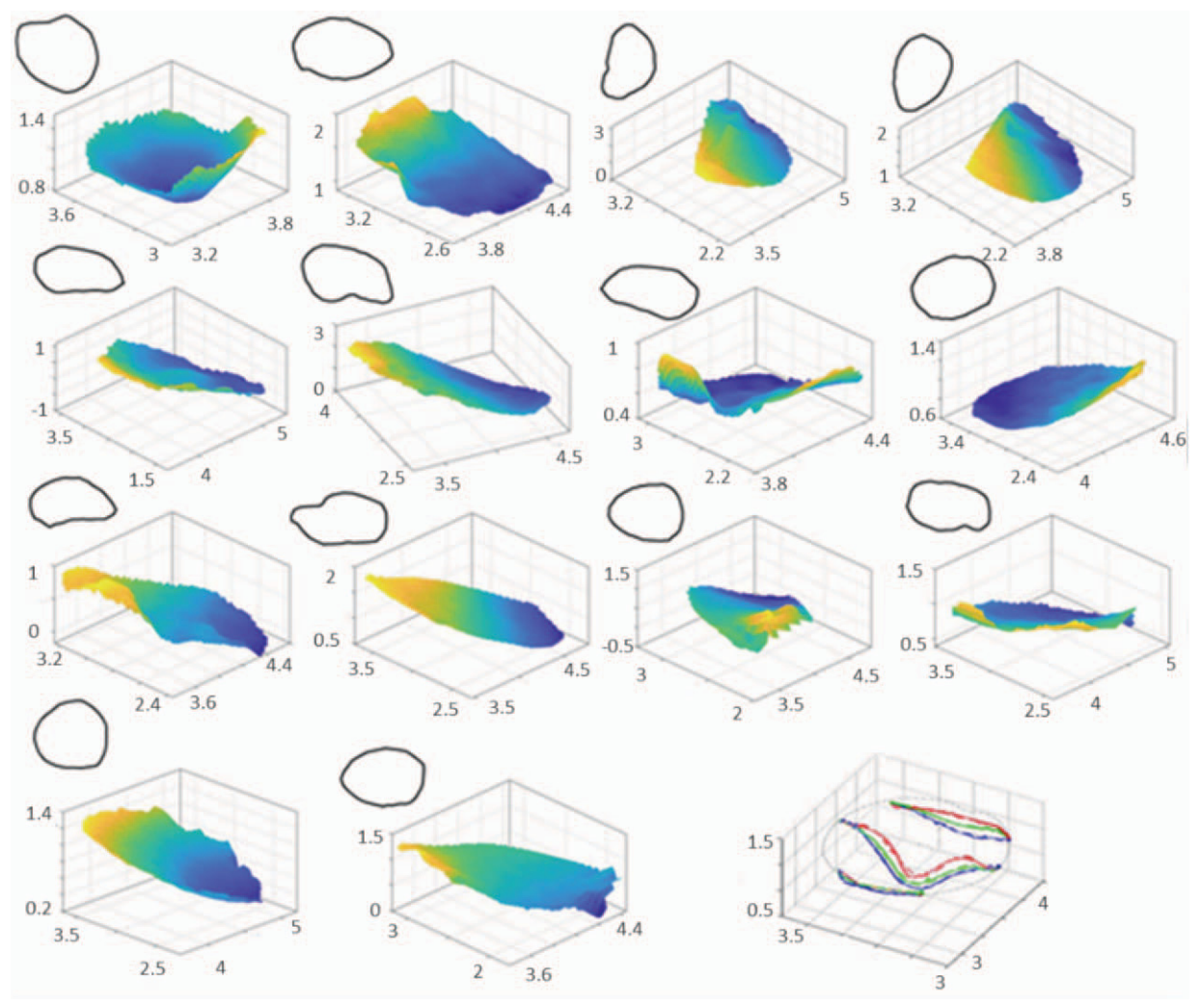


FIG. 3. 3D surface of 14 RWM reconstructed from micro-fringe projection. The shapes of the RW from medial views are plotted on top of each 3D surface. The right bottom plot demonstrates the curve fitting between FE simulated (*solid line*) and experimental measured profiles (*dash line*) of three pressures at three cross-sections. FE indicates finite element; RWM, round window membrane.

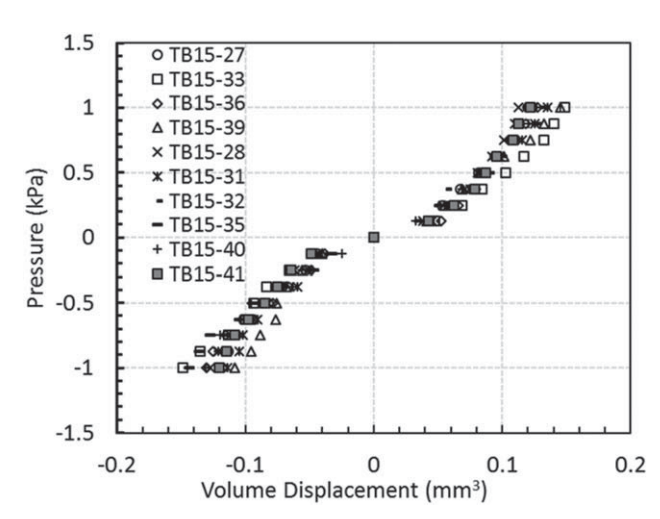


FIG. 4. Pressure–volume displacement relationship of 14 RWM. RWM indicates round window membrane.

from another study on human temporal bone conducted by Ivarsson and Pedersen (14).

The parameters μ_i and α_i from the inverse method are listed in Table 1, with which, uniaxial stress-strain relationship and the tangent modulus-strain relationship of RWM can be obtained. Figure 5A shows the uniaxial stress-strain relationship of the 14 RWM samples up to the maximum strain (0.32, which is determined from the FE simulation). The uniaxial stress-strain curve of the RWM, also exhibits a strong nonlinearity. The stress has an approximate linear section when the strain is below 5%, then the increase rate of stress continues descending. Correspondingly, tangent modulus exhibits a continuous decrease and approaching a constant value as shown in Figure 5B. At a strain close to zero, the average tangent modulus is 2.48 MPa, and slightly decreases to 1.30 MPa at 30% strain. The average Young's modulus of the 14 RWM is approximately 1.98 MPa.

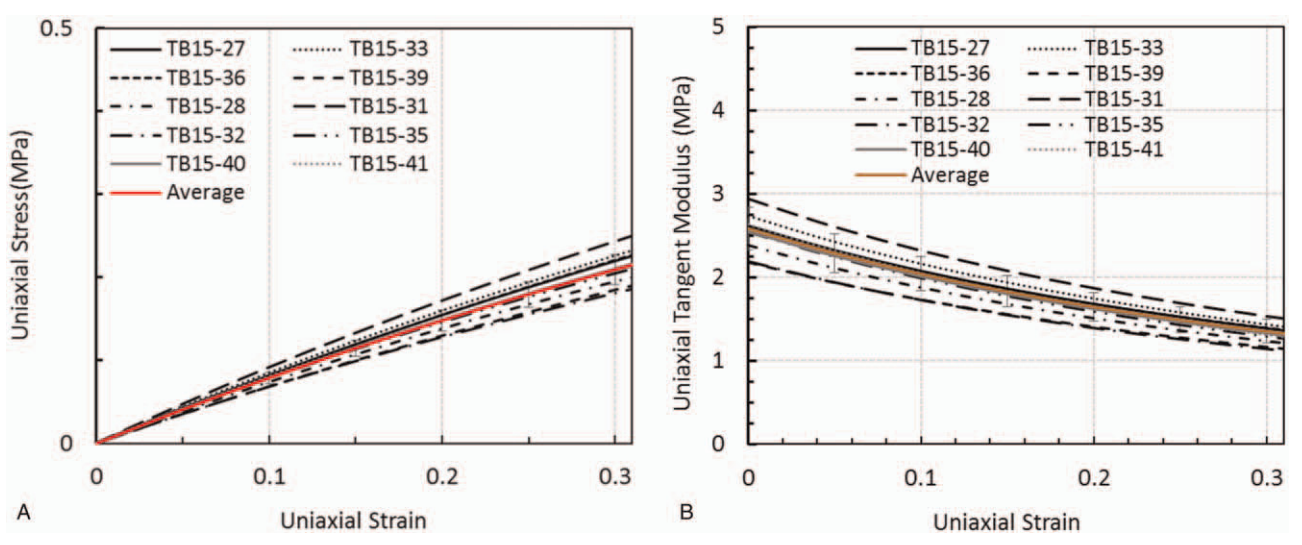


FIG. 5. Mechanical properties determined through the inverse problem solving (*A*) stress–strain relationship for 14 human RWMs. (*B*) Tangent modulus for 14 human RWMs derived from the stress–strain relationship. RWM indicates round window membrane.

DISCUSSION

Micro-fringe projection was proven to be a very effective method to measure the surface topography of RWM with microscopic precision for geometrical analysis. The 3-D geometry of the RWM can be clearly established and the variations and irregular geometry of the human RWM can be observed. The commonest observed shape was an oval-shaped membrane (35.7%) while a pear shape was scarcely seen in two (14.3%) cases. To date, there is no empirical evidence that shows the direct relationship between the geometry of RW and the surface geometry of RWM. In this study, we focus on the geometry and the mechanical properties only of the RWM. The entrance of the RW and its niche was used as a small conceal compartment to applied air pressure to the RWM for mechanical properties measurement. The RWM was exposed from the cochlear side and most of the RW niche on this side was removed to enable the full observation of the RWM. Therefore, the RW geometry is not considered.

Histologically or anatomically, it was difficult to define a plane for RWM because of the out-of-plane geometry and irregular outline. Previous anatomic studies of the RWM have shown the combination of the concave and convex surface structure of the RWM and its similarity to "Pringels potato chip" (2,26-28) convex toward the cochlea (22,29). The curvature was reported as around 0.1 mm⁻¹ (30,31). However, the 3D reconstruction of RWMs surface in this study shows that there is no conclusive pattern associated with the convexity. Meanwhile, a surprisingly large variation in curvature values is found ranging from 0.3 to 3.76 mm⁻¹. Such a large size variation is also against the conclusion about RWM curvature of 0.1 mm⁻¹. It implies that the physiologic function of RWM is not, to a major degree. dependent on its convexity. This finding is important for cochlea implant design. Practically, cochlear implant electrode arrays inserted through the RW are frequently found to partially reshape the curvature of RWM (32). The finding from the RWM curvature variety indicates that the RMW convexity alternation is unlikely to be responsible for the increased low-frequency tone thresholds observed after surgery (33).

Although the convexity of the RWM may not have a significant impact on the physiologic function, its curvature, however, can be crucial for the design of floating mass transducer (FMT) because numerous publications show that the successful function of coupling strongly relies on the knowledge of the geometry of RMW (6,7,34,35). The anatomy of RWM has direct implication for the design of FMT. An FMT must be designed to maximize the energy transfer efficacy to the perilymph fluid and minimize the stress within the RWM to minimize the possibility of rupturing the RWM because of repetitive extension and contraction of the membrane. The convexity of the RWM determines the surface tension of the RWM and the contact between the FMT and RWM. However, RWM are commonly simulated as with a flat ellipse surface in FMT simulation (13,36) and inverse problem (16). Watanabe et al. (37) already show that modifying the convexity of RWM can cause a difference in determining Young's modulus from inverse method up to 40%. The detailed RWM topography data measured in this study can potentially improve the FE model for designing FMT and in determining mechanical behavior of RWM using inverse method.

Reported data on the mechanical properties of RWM in the literature are notably rare. To our knowledge, most of the mechanical properties used in the FE modeling were indirectly determined based on the validation from the model (For instance Gan et al. (12) and Kwacz et al. (38)). The only direct measured mechanical properties reported in the literature are those from the indentation

test (15), the dynamic mechanical testing (16,17), and from the nano-indentation test (37). Mechanical properties of RWM reported in our work are the only data from an in situ measurement. The results here show that the mechanical response of RWM is highly nonlinear, which behaves similarly to that of rubber. The average young's modulus of the RWM is 1.98 MPa. This result is comparable to the dynamic properties at low frequency measured using dynamic mechanical testing (1.35-2.22 MPa) reported by Zhang and Gan. However, our results are one magnitude smaller than those reported by Watanabe et al. (37). In Watanabe's work, a similar inverse problem solving scheme was used to determine the mechanical properties from the experimental nanoindentation results. The difference between our results and Watanabe's results may stem from the fact that the RWM was assumed to be elastic in Watanabe's model, which can overestimate the stiffness of the material properties out of the elastic range of the material.

Both geometry and mechanical properties of RWM are important information for cochlear implantation surgery and FTM design. As observed in this study, while the mechanical properties do not differ significantly among the individual RWM, the surface geometries exhibit a remarkably large variation. Surgery or transducer designed based on statistic parameters from general surface profile data may not yield a satisfactory outcome on hearing rehabilitation for individuals. In this study, we explored an optical method, micro-fringe projection to reconstruct the 3D surface in situ for individual RWM. In the future, this experimental setup can be replaced with more practical clinical tools such as a confocal microscope or computational tomography to determine the surface in vivo. The method of combination of using general RWM mechanical properties and individual RWM geometries will potentially allow customize cochlear implantation and FMT coupling design, which will improve the quality of clinical outcomes.

CONCLUSION

Geometries and mechanical properties of RWM were measured using a micro-fringe projection technique. FE models of RWM were created, with which, an inverse method was used to determine the mechanical properties of RWM by fitting the simulated pressure-volume displacement with the experimental results. The geometries of RWM were found to be non-planar and exhibit large variation in terms of convexity. The curvatures of the RWM surface vary along both long and short axis making RWM a commonly saddle-like shape. The tangent modulus of RWM, non-linearly decreases with the stress. The average Young's modulus of RWM is about 1.98 MPa. The data in this study can potentially be used for building highly realistic FE models of human ear, for assisting cochlear implantation surgery and for designing new generation RWM FMT.

Acknowledgments: The authors acknowledge the support of DOD W81XWH-14-1-0228, NIH R01DC011585, DOD

W81XWH-13-MOMJPC5-IPPEHA, and NSF CMMI-1636306, CMMI-1661246, and CMMI-172043. They also acknowledges the Louis A. Beecherl Jr. Chair for additional support.

REFERENCES

- Hellstrom S, Eriksson PO, Yoon YJ, et al. Interactions between the middle ear and the inner ear: bacterial products. *Ann N Y Acad Sci* 1997:830:110-9.
- Nomura Y. Otological significance of the round window. Adv Otorhinolaryngol 1984;33:1–162.
- Paparella MM, Schachern PA, Choo YB. The round window membrane: otological observations. *Ann Otol Rhinol Laryngol* 1983:92:629–34.
- Scarpa A. Anatomicae Observationes de Structura Fenestrae Rotundae et de Tympano Secundario. Modena, MA: Typographicam Societatum; 1772.
- Adunka O, Unkelbach MH, Mack M, et al. Cochlear implantation via the round window membrane minimizes trauma to cochlear structures: a histologically controlled insertion study. *Acta Otolar-yngol* 2004;124:807–12.
- Gostian AO, Pazen D, Ortmann M, et al. Loads and coupling modalities influence the performance of the floating mass transducer as a round window driver. *Otol Neurotol* 2016;37:524–32.
- Gostian AO, Schwarz D, Mandt P, et al. Performance of the round window soft coupler for the backward stimulation of the cochlea in a temporal bone model. *Eur Arch Otorhinolaryngol* 2016; 273:3651–61.
- 8. Arnold A, Kompis M, Candreia C, et al. The floating mass transducer at the round window: direct transmission or bone conduction? *Hear Res* 2010;263:120–7.
- Arnold A, Stieger C, Candreia C, et al. Factors improving the vibration transfer of the floating mass transducer at the round window. *Otol Neurotol* 2010;31:122–8.
- Beltrame AM, Martini A, Prosser S, et al. Coupling the Vibrant Soundbridge to cochlea round window: auditory results in patients with mixed hearing loss. *Otol Neurotol* 2009;30:194–201.
- Bohnke F, Arnold W. 3D-finite element model of the human cochlea including fluid-structure couplings. ORL J Otorhinolaryngol Relat Spec 1999;61:305–10.
- 12. Gan RZ, Reeves BP, Wang X. Modeling of sound transmission from ear canal to cochlea. *Ann Biomed Eng* 2007;35:2180–95.
- 13. Zhang X, Gan RZ. A comprehensive model of human ear for analysis of implantable hearing devices. *IEEE Trans Biomed Eng* 2011;58:3024–7.
- Ivarsson A, Pedersen K. Volume-pressure properties of round and oval windows. A quantitative study on human temporal bone. *Acta Otolaryngol* 1977;84:38–43.
- Ishii T, Takayama M, Takahashi Y. Mechanical properties of human round window, basilar and Reissner's membranes. Acta Otolaryngol Suppl 1995;519:78–82.
- Zhang X, Gan RZ. Dynamic properties of human round window membrane in auditory frequencies running head: dynamic properties of round window membrane. Med Eng Phys 2013;35:310–8.
- 17. Gan RZ, Nakmali D, Zhang X. Dynamic properties of round window membrane in guinea pig otitis media model measured with electromagnetic stimulation. *Hear Res* 2013;301:125–36.
- Ortiz M, Patterson EA. On the industrial applications of moire and fringe projection techniques. Strain 2003;39:95–100.
- Ortiz MH, Patterson EA. Location and shape measurement using a portable fringe projection system. Exp Mech 2005;45:197–204.
- Liang J, Fu B, Luo H, et al. Characterization the nonlinear elastic behavior of guinea pig tympanic membrane using micro-fringe projection. *Int J Exp Comput Biomech* 2015;3:319–44.
- 21. Liang JF, Luo HY, Yokell Z, et al. Characterization of the nonlinear elastic behavior of chinchilla tympanic membrane using microfringe projection. *Hear Res* 2016;339:1–11.
- Goycoolea MV, Lundman L. Round window membrane. Structure function and permeability: a review. *Microsc Res Tech* 1997; 36:201–11.

- Sahni RS, Paparella MM, Schachern PA, et al. Thickness of the human round window membrane in different forms of otitis media. *Arch Otolaryngol Head Neck Surg* 1987;113:630–4.
- Atturo F, Barbara M, Rask-Andersen H. Is the human round window really round? An anatomic study with surgical implications. Otol Neurotol 2014;35:1354–60.
- Kumar R, Singh A, Sagar P, et al. Access to round window niche via posterior tympanotomy and impact of drilling its overhangs: a cadaveric descriptive study. *Indian J Otolaryngol Head Neck Surg* 2018;70:510–4.
- Proctor B, Bollobas B, Niparko JK. Anatomy of the round window niche. Ann Otol Rhinol Laryngol 1986;95:444–6.
- Watanabe H, Kysar JW, Lalwani AK. Microanatomic analysis of the round window membrane by white light interferometry and microcomputed tomography for mechanical amplification. *Otol Neurotol* 2014;35:672–8.
- Rask-Andersen H, Kinnefors A, Svedberg M, et al. The human round window-a perilymph pressure regulator? On a novel mechanoreceptor-like neuron in the human round window membrane. *Audiol Med* 2004;3:182–92.
- Carpenter AM, Muchow D, Goycoolea MV. Ultrastructural studies of the human round window membrane. Arch Otolaryngol Head Neck Surg 1989;115:585–90.
- Li PM, Wang H, Northrop C, et al. Anatomy of the round window and hook region of the cochlea with implications for cochlear implantation and other endocochlear surgical procedures. *Otol Neurotol* 2007;28:641–8.

- Toth M, Alpar A, Patonay L, et al. Development and surgical anatomy of the round window niche. Ann Anat 2006;188:93–101.
- Adunka OF, Dillon MT, Adunka MC, et al. Hearing preservation and speech perception outcomes with electric-acoustic stimulation after 12 months of listening experience. *Laryngoscope* 2013; 123:2509–15.
- D'Hondt C, Wouters J, Verhaert N. Alteration of the relative vibration of the round window membrane after implantation of a direct acoustic cochlear implant. *Int J Audiol* 2019;59:341–7.
- 34. Gostian AO, Pazen D, Ortmann M, et al. Impact of coupling techiniques of an active middle ear device to the round window membrane for the backward stimulation of cochlea. *Otol Neurotol* 2014;36:111-7.
- Olszewski L, Jedrzejczak WW, Piotrowska A, et al. Round window stimulation with the Vibrant Soundbridge: comparison of direct and indirect coupling. *Laryngoscope* 2017;127:2843–9.
- 36. Tian JB, Huang XS, Rao ZS, et al. Finite element analysis of the effect of actuator coupling conditions on round window stimulation. *J Mech Med Biol* 2015;15:1550048.
- Watanabe H, Lalwani AK, Kysar JW. In situ nano-indentation of round window membrane. Conference Proceedings of the Society for Experimental Mechanics Series. The Society for Experimental Mechanics, Inc., 2016.
- Kwacz M, Marek P, Borkowski P, Mrowka M. A three-dimensional finite element model of round window membrane vibration before and after stapedotomy surgery. *Biomech Model Mechanobiol* 2013;12:1243–61.